JST: Engineering and Technology for Sustainable Development
Volume 33, Issue 5, November 2023, 001-008

Effects of Hybrid Diffuser in Axial-Flow Jet Engine Combustor

Cong-Truong Dinh*, Trong-Nghia Hoang, Xuan-Truong Le, Van-Minh Le, Phuong-Nam Nguyen
Hanoi University of Science and Technology, Ha Noi, Vietnam
**Corresponding author email: truong.dinhcong@hust.edu.vn*

Abstract

It is believed that the turbine engine plays a vital role in the performance of aircraft. Most jet engines nowadays use the axial compressor. In axial-flow compressors, the rising pressure through each stage is dependent on the axial flow velocity. A high axial velocity is essential to achieve the design pressure with the minimum number of stages. Thus, before the combustion can proceed, the air velocity must be reduced to about 20% of the compressor outlet velocity. This depletion is accomplished by fitting a diffuser between the compressor outlet and the upstream end of the liner. Throughout much research into diffuser performance, it has been shown that the operation depends particularly on the flow. Besides, there are several problems that could result in the loss of its efficiency. This study will focus on increasing the diffuser performance of a hybrid type one via pressure-recovery coefficient C_p and loss coefficient λ.

Keywords: Jet engine combustion, hybrid diffuser, RANS analysis, diffuser performance.

1. Introduction

The diffuser is the divergent section of the engine after the compressor and before the combustion section. It has the all-important function of reducing high-velocity compressor discharge air to increased pressure at a slower velocity. Compressor outlet velocities may reach 170 m/s or higher in many aircraft engines. It is impossible to attempt to burn fuels in the air flowing at such high velocities because the air has no time to catch fire so the ignition process cannot be achieved. The diffuser prepares the air for entry into the flame-burning area of the combustion section at a lower velocity so that the flame of combustion can burn continuously. If the air passes through the flame area at a high velocity, it could extinguish the flame.

The performance of the diffuser is influenced not only by geometry but also by other characteristics. Klein [1] reported that the Reynolds number has no effect on the performance of a conical diffuser and indicates that the Reynolds number is a relatively weak parameter if the flow at the inlet is fully turbulent. Stevens and Williams [2] found that the turbulence produced in a long approach duct has a beneficial effect on diffuser performance as it reduces the distortions in the flow. Normally the flow from the last stage compressor is not lamina flow, the turbulence factor effects greatly the diffuser's behaviours, some have negative, but some have a positive effect.

In the axial compressor, the air is pressured by the rotating and stating blade which causes the flow to exit the compressor to have some degree of swirl. A lot of experimental studies have been carried out to analyse the effect of swirl angles on diffuser performance. Liepe [3] found that the addition of a whirl velocity component to an otherwise axial flow in a conical diffuser can lead to improvements in static pressure recovery and efficiency. Diffusers of total conical angles 10, 20, and 30 degrees were tested in detail. Improvements were evident only in the last two, which would otherwise have suffered from flow separation problems caused by their relatively large divergence angles. The agency for improvement seems to be a beneficial redistribution of axial velocities. Elkersh *et al.* [4] studied the influence of geometrical parameters and swirls on the performance of equiangular diffusers by testing three diffusers over a range of inlet swirls up to 45°, and the swirls being of free vortex distribution. The data indicate similar flow patterns for different cant angles, and the centrifugal forces due to the swirl stabilize the flow on the outer wall while increasing the tendency towards separation at the inner wall. Diffuser performance improves as the inlet swirl increases up to 30°, the improvement being influenced by area ratio and cant angle. A further increase of swirl causes a deterioration of performance. The effect of the inlet swirl on the condition of the boundary layers is demonstrated. Hanna *et al.* [5] reported that the experimental results showed significant changes in the velocity profiles with the wake-flow inlet. The peak velocities for the fully developed turbulent flow case diverge towards the centreline of the diffuser. However, in the case of wake flow, the peak velocities are prevailing in the region close to the straight wall of the diffuser. The influence of the wake flow leads to deterioration of the

ISSN 2734-9381
https://doi.org/10.51316/jst.170.etsd.2023.33.5.1
Received: April 20, 2022; accepted: August 9, 2023

static pressure recovery coefficient and increases the total pressure loss coefficient of the diffuser.

The hybrid diffuser is a new concept the diffuser which brings more benefits to the performance criteria. In other words, it could create a higher pressure-recovery coefficient and lower pressure loss coefficient. Adkins *et al.* [6] demonstrated that the hybrid diffuser has great potential. It is compact, half the length of the equivalent conical diffuser, and would operate satisfactorily without either bleed-off or vanes projecting into the flow. It can produce high levels of pressure recovery, both with and without external suction being applied. With suction, it matches the pressure recovery of the extremely efficient vortex-controlled diffuser when constrained to the same. Without suction being applied, the diffuser produced pressure recoveries that were 25 percent higher than those obtainable from the optimum design of conventional divergent ducts having the same length. Furthermore, Juhasz [7] conducted a performance test on a short dump annular diffuser equipped with suction capability through peripheral edge slots on both the inner and outer diffuser walls. Some performance improvement was also obtained with suction, as indicated by a rise in diffuser effectiveness from 25 percent with no suction to 50 percent at 6 percent outer-wall suction and to 52.6 percent at a combined suction rate of 10.25 percent on both walls. At the same time, the diffuser's total pressure loss was reduced by approximately one-fourth. Diffuser performance was found to be better with tip-biased than with hub-biased exit velocity profiles. Verdouw [8] studied the performance of the vortex-controlled annular combustor diffuser and reported high-pressure recovery and very low-pressure loss using vortex-controlled diffuser fences.

Adkins and Wardle [9] have shown their hybrid diffuser by creating a vortex chamber to control the bleeding air. However, this shape is impractical since it requires a lot of space, increasing the weight. Walker *et al.* [10] demonstrated the operation of a hybrid diffuser within an isothermal representation of a modern gas turbine combustion system. Compared to a conventional single-passage pre-diffuser the hybrid diffuser achieved a significant increase in area ratio within the same axial length. Moreover, the increased area ratio resulted in an improved diffuser static pressure recovery, reducing total pressure losses in the dump cavity and to the feed annuli. The required level of bleed was found to be similar to that used for turbine blade cooling and measurements suggested that the bleed air would be of sufficient quality.

When researching about diffuser performance, it has been shown that the diffuser operation depends greatly on the flow. In addition, there are several problems with the flow inside the diffuser which could cause loss and efficient reduction. This paper will focus on increasing its performance by using a hybrid diffuser.

2. Numerical Analysis

2.1. Design Description

Following the basic design, the study uses a diffuser geometry that has been researched before: The plane diffuser experiment by Obi *et al.* [11], which has fully developed inlet conditions and includes separation from a smooth wall, subsequent reattachment, and redevelopment of the downstream boundary layer. The summary geometry is shown in Fig. 1.

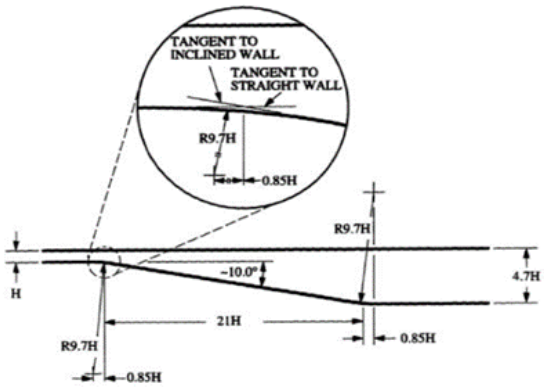

Fig. 1. Schematic design of the diffuser.

Table 1. Diffuser Geometry

Main parameters	Value
Inlet	1.5 (cm)
Outlet	7.05 (cm)
Length	31.5 (cm)
Angle	10°

In Table. 1, H is the fundamental parameter for Inlet length since they are all dependent on H. The area ratio of the diffuser is high compared to other diffusers in aircraft engines, which is 4.7. In addition, Obi's diffuser is flat which means the design is built in 2D. The wind tubes before and after the diffuser inlet and outlet were also created. In experimental design, H is 1.5 cm.

The performance of the diffuser in 3D annulus shape is also discussed, as shown in Fig. 2. The 2D diffuser is transformed and converted into 3D annulus type by rotating its geometry around the Ox axis with radius $R = 45\ cm$. Although the diffuser is annulus which means 360 degrees, in the simulation, we only investigate up to 30 degrees. Parameters of the bleeding tube are illustrated in Fig. 3, with X being the distance between the inlet and the bleeding tube, and

W being the bleeding tube's width. Those are chosen to be proportional to *H* for the non-dimensionless parameters study later. A 3D bleeding tube is created in the same way as the 2D diffuser. It has 4 important parameters: α, bleed rate, *X*, and *W*. *X* and *W* have been mentioned before, α is the angle of the tube, and bleed rate is the mass flow through the bleeding tube. They are shown in Table. 2.

Table 2. Bleeding tube Geometry

Unit	Value
A (=*A*16)	90°
X (=*H*15)	15 (cm)
W (=*H*14)	0.75 (cm)
*V*17	12 (cm)

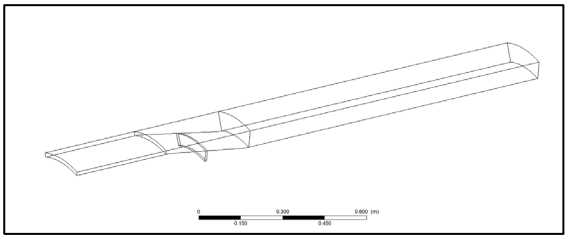

Fig. 2. 3D Geometry of the diffuser

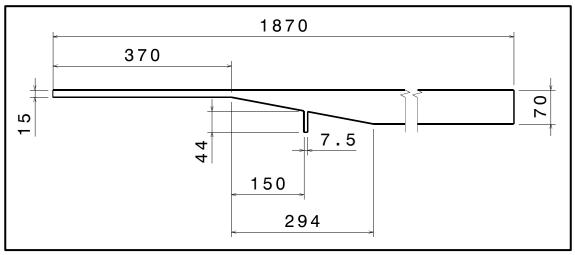

Fig. 3. 2D Geometry of the diffuser (Unit: mm)

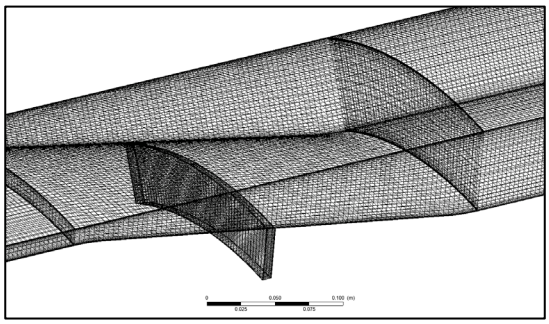

Fig. 4. Energy conversion in a diffuser

Considering the injector at the eighth hole with the cross-section between the nozzles, the effect of the circular cavity on combustion performance is also included. All holes have a radius of 15 mm and they are put after the wedge strut. Distances between holes and inlet are *x* (80 mm< *x* < 260 mm).

The pressure-recovery coefficient (C_p), which shows the relative static pressure between inlet and outlet of the diffuser, is calculated as:

$$C_p = \frac{p_2 - p_1}{q_1} \quad (1)$$

In an ideal diffuser that has no losses:

$$(p_2 - p_1)_{ideal} = q_1\left(1 - \frac{1}{AR^2}\right) \quad (2)$$

A non-dimensional coefficient of ideal static pressure rises, $C_{p_{ideal}}$, is derived from (2) to become:

$$C_{p_{ideal}} = (p_2 - p_1)_{ideal}/q_1 = \left(1 - \frac{1}{AR^2}\right) \quad (3)$$

Loss coefficient (λ) is defined as:

$$\lambda = \frac{P_1 - P_2}{q_1} \quad (4)$$

2.2. Numerical Method

In the study, three-dimensional RANS equations using the SST turbulence model were solved numerically using the commercial software ANSYS 19.1 [12]. In the mesh part created by ANSYS ICEM, the first boundary layer was 1e-05, which is a suitable value of y^+ for the SST model. Fig. 5 illustrates the mesh of the main diffuser. The bleeding tube is meshed separately. The value of the first layer is also 1e-05.

The inlet condition was specified as a constant velocity profile corresponding to $v = 20$ m/s. The outlet was chosen at 0 Pa with static pressure. The boundary condition for the bleeding tube outlet is 3.52e-3 mass flow rate, calculated at 4% of the mass flow inlet. The fluid density is 1.225 kg/m^3 and the dynamic viscosity is selected to be 1.789*x*1e-05 kg/ms. The simulation uses SST model to fit with other works that have been done before.

In all cases, corresponding calculation residuals are monitored to converge at 1e-05. These residuals included continuity, *x*-velocity, and *y*-velocity for all turbulence models.

Typical values of λ range from around 0.15 to 0.45 for dump diffusers with a high liner/depth ratio (D_l/h_l). For vortex-controlled diffusers (VCD), reported values of λ range from 0.05 to 0.15.

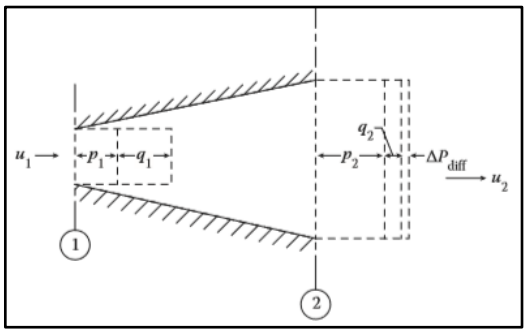

Fig. 5. 3D Mesh of the diffuser with a bleeding tube

In the solution case, residuals are controlled and the C_p and λ are plotted to justify the convergence of the solution. After 300 interactions (about 1.5 hour), the curve of C_p and λ remains constant, and the solution is converged.

3. Result and Discussion

3.1. Grid Independence and Validation Results

The pressure coefficient validates with the experimental data provided by Chandavari and Palekar [13] to prove the precision of geometry and numerical method. Four mesh models were applied in the simulation of the diffuser to find out the optimal value. The number of nodes and elements increases one by one: 1, 2, 3, and 4 with 2540, 10200, 20200, and 30100 respectively. Fig. 6 illustrates the graph of (C_p-mesh nodes) with 2 lines: *x*/*H*=10 and *x*/*H*=27. They are in the same kind of pattern and are used to compare the statistical results. After the third point in both lines, the optimal value of C_p is reached and becomes stabilized at 300,000 nodes. Moreover, after mesh 3 (20200 nodes), the results show the same in both points, so mesh 3 is the optimal mesh. Fig. 7 points up and emphasizes the similarity between the experimental and modelling data of the hybrid diffuser. They look alike without any significant differences except the extent of value at the initiation of the computing process, which can be understood by varied results that come from some very first iterations.

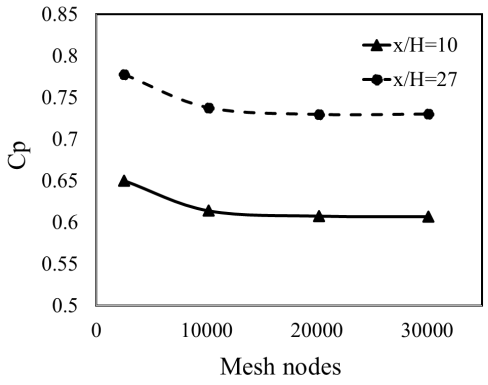

Fig. 6. Mesh convergence

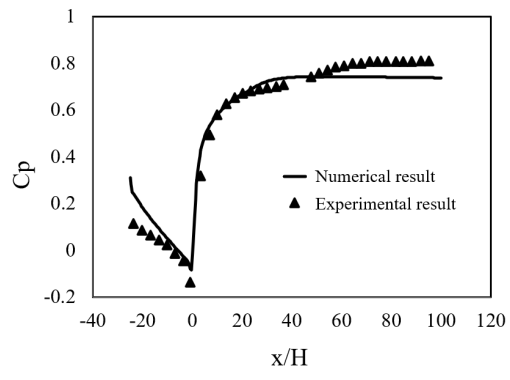

Fig. 7. Validation result of C_p

Table 3. Design values of bleed tube parameters

Main parameters	Value
Bleed rate	4%
Distance	10*H*
Width	0.5*H*
Angle	90°

Table 4. Mesh convergence for Diffuser with bleed tube

Mesh	Bleed tube nodes number	*Cp* (at *x*/*H*=10)
Mesh1	2000	0.662101
Mesh2	4000	0.666242
Mesh3	6000	0.667141
Mesh4	8000	0.667351

The bleed tube design values were selected as shown in Table 3, where the bleed rate and angle with the diffuser axis direction were selected at 4% of inlet mass flow rate and 90°, respectively. The numerical result of *Cp* at the line of *x*/*H*=10 is presented in Table 4, where the Mesh 3 (6000 nodes) shows that the value of *Cp* at the line of *x*/*H*=10 is almost constant, and Mesh 3 is selected for the bleed tube optimal mesh.

3.2. Parameters study

Parameters study focuses on examining the influence of the bleeding tube on the diffuser performance, specifically about the static pressure loss coefficient C_p and the loss coefficient λ. In addition, four main parameters (Table 3) have been analysed and only one of them needed to change, while others remain the same. Table 5 presents all bleed tube parameters, which are all non-dimensional quantities.

Table 5. The changes in bleed tube parameters

Main parameters	Lower value	Upper value
Bleed rate	1%	9%
Distance	2.5*H*	15*H*
Width	0.4*H*	0.8*H*
Angle	30°	120°

3.2.1. Effect of the bleed rate

Fig. 8a clarified that the static pressure recovery coefficient has a weighty increase. Without any bleeding tube within the diffuser, the value of C_p is only equal to 0.64. In contrast, in case it has one, C_p raises rapidly to 0.682 at 5% of the mass flow bleed rate. There is a 6.6% gain in the pressure recovery coefficient, which means the overall performance is also enhanced by 6.6 %. However, if we keep soaring

the bleed rate, the value of C_p will shrink. At a 9% bleeding rate, the pressure recovery coefficient falls to 0.672, but it's still higher than the case without a bleeding tube. Therefore, by all accounts, it leads to a conclusion: inflating the bleed rate brings no benefit but in reverse it makes the operation of the diffuser become less effective, and anyway, losing a part of the main flow is not good for the overall performance. In Fig. 8b, it is apparent that the pressure coefficient loss λ declines gradually along with the bleed rate increment, in opposition to the case of the pressure recovery coefficient. But after being reduced to 0.155 at 5% bleed rate, the value seems stable and only drops a little more. For the most part, the reduction of λ shows great potential as it lessens the pressure loss from 0.19 to 0.155 at 5%, which is an 18.42% improvement.

As shown in Fig. 9, the flow separates underneath the diffuser due to the Coanda principle. Vortices are created in regions that have low horizontal velocities. By inserting a bleeding tube, it could extract the swirling and increase the diffuser performance. The more vortices are taken, the better the effectiveness turned out to be. This is accomplished by raising the bleed rate value and using the bleeding tube to direct the flow toward the bottommost of the wall. Nevertheless, if the bleed rate is too high, it may affect the upper boundary and creates new vortices around that region.

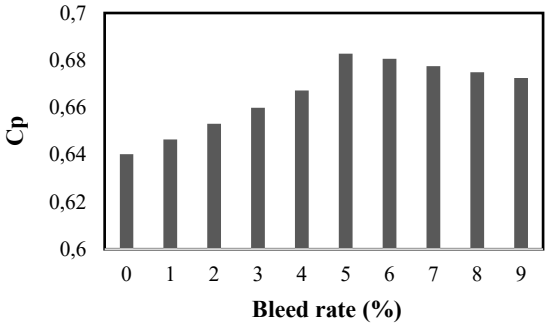

(a) C_p versus bleed rate

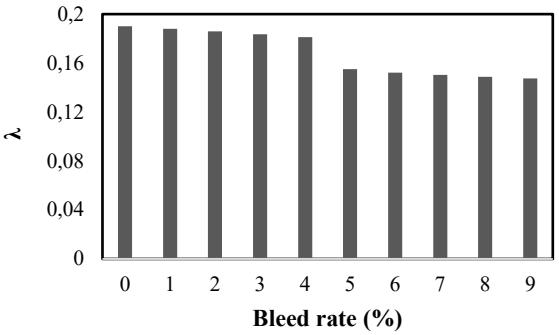

(b) λ versus bleed rate

Fig. 8. Effect of the bleed rate

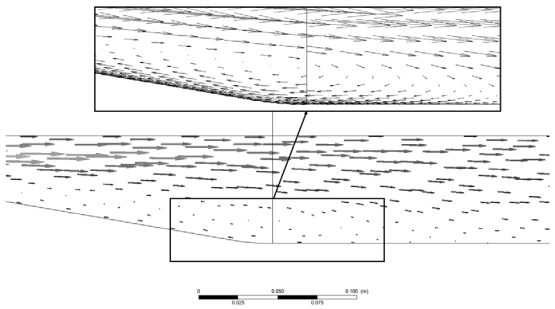

(a) Without a bleeding tube

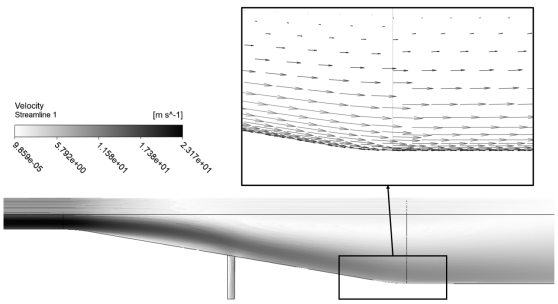

(b) With a bleeding tube

Fig. 9. Streamlines distribution and velocity profile in the diffuser with and without a bleeding tube

3.2.2. Effect of the bleeding tube width

The value of static pressure recovery C_p and total pressure loss λ are verified with the width parameter. Fig. 10 shows that changing the width of the bleeding tube can affect the value of C_p and λ. From the chart, the value of C_p is highest at $0.6H$ and $0.7H$, equal to 0.685, which means 7% higher than the diffuser with no bleed. Total pressure loss λ also achieves the lowest value, 16% decreased, at the same width range as C_p. This could be explained that the vortex near the wall is smaller as shown in Fig. 11 compared to the case of no bleed.

3.2.3. Effect of the distance from the inlet

The distance of the bleeding tube from the inlet of the diffuser is an important factor. To cover the whole length of the diffuser, it is chosen at $2.5H$. The performance criteria are studied in 6 cases: $2.5H$, $5H$, $7.5H$, $10H$, $12.5H$, and $15H$. C_p and λ are plotted in Fig. 12(a, b).

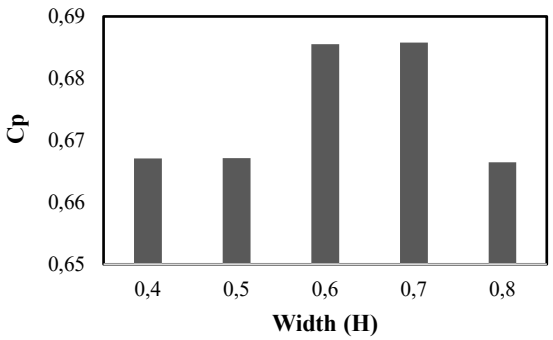

(a) C_p versus the width of the bleeding tube

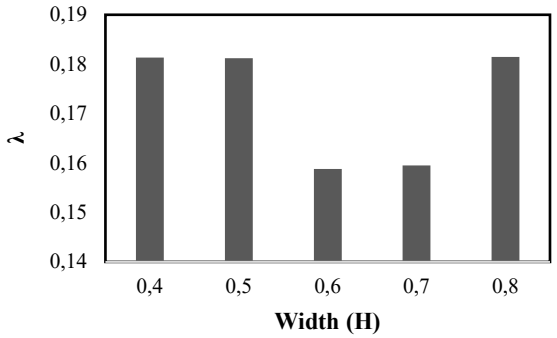

(b) λ versus the width of the bleeding tube

Fig. 10. Effect of the bleeding tube's width

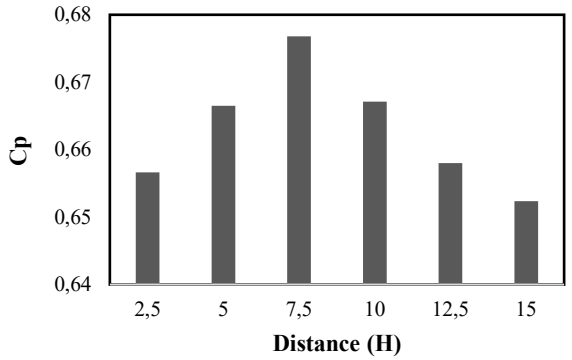

(a) C_p versus the distance from the inlet

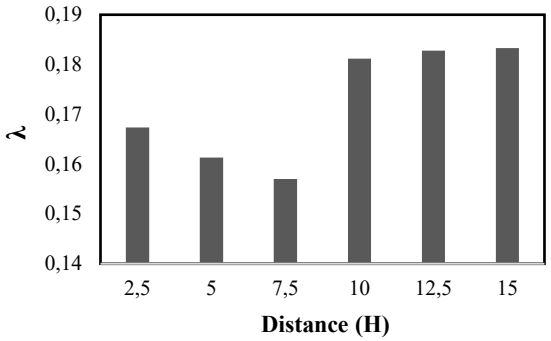

(b) λ versus the distance from the inlet

Fig. 12. Effect of distances of the bleeding tube counted from the inlet.

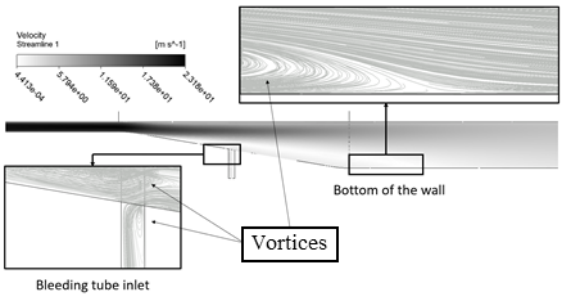

Fig. 11. Streamlines distribution and velocity profile of the diffuser with a 0.6H-width bleeding tube

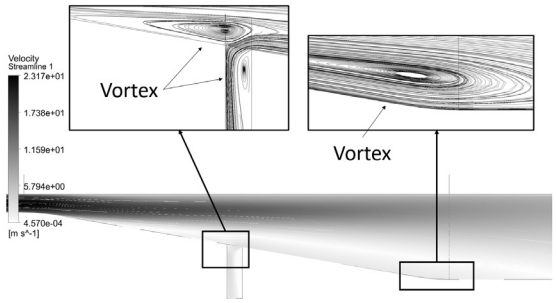

Fig. 13. Streamlines distribution shows recirculation regions near bleeding tube and bottom wall at a distance of 7.5H from the diffuser inlet.

In Fig. 12a, C_p reaches the maximum value at the distance of 7.5H, others are lower. The opposite phenomenon happened in Fig. 11b when λ reaches the minimum value at 7.5H. Then obviously 7.5H is the distance that has the best performance criteria. It could be explained when the flow separates at approximately 3H following the Z direction, the bleeding tube extracts more flow around that region. But the diffuser performance in this case is lower compared to others (Fig.13). Notably, the 7.5H distance is not a suitable position for a bleeding tube to be placed, but it diminishes most of the influence of the vortex.

3.2.4. Effect of the angle of the bleeding tube

There are 5 cases including different angles that have been used. The changes in pressure recovery coefficient and pressure loss are shown in Fig. 14(a) and (b). It is obvious that augmenting the angle of the bleeding tube isn't always come along with a good result. The static pressure recovery coefficient C_p decreases significantly from 0.686 to 0.64 when the angle of the bleeding tube increases, and the pressure loss coefficient λ also rises from 0.15 to 0.19, which is 26.67% worst. Apart from that, there is a bleeding tube

angle value which simultaneously gives a rise to C_p while reducing λ. It happened at 45 degrees.

With small angles, the vortex in the Coanda bubble seems to bleed more than usual. In Fig. 15, it is extracted following the downstream of the bleeding tube. Usually, the vortex reduces the influence of flow separation on the performance of the diffuser. However, in the case of large angles, the flow is harder to bleed out, and as a result, there are still many vortices existing at the bottom of the wall.

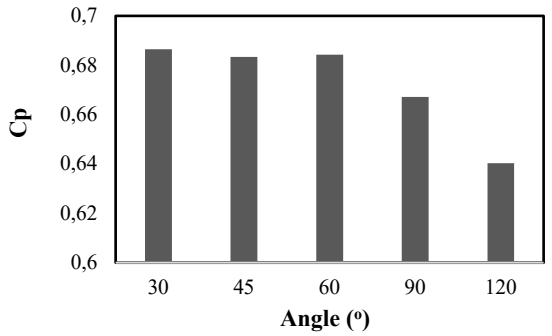

(a) C_p versus the angle of the bleeding tube

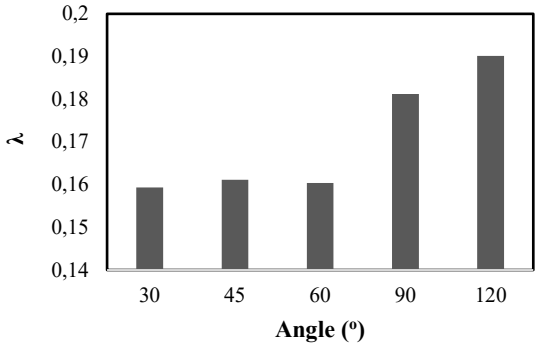

(b) λ versus the angle of the bleeding tube

Fig. 14. Effect of the bleeding tube angles on C_p and λ

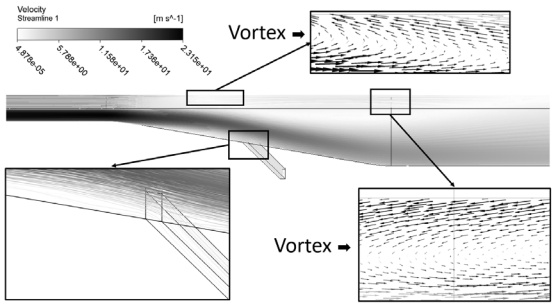

(a) Velocity profile with a 45-degree backward-leaned bleeding tube

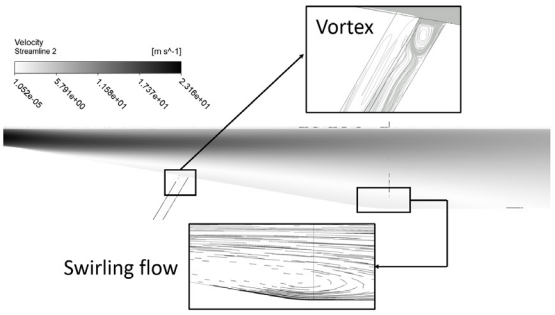

(b) Streamline distribution shows vortices at the inlet of 120-degree forward-leaned bleeding tube

Fig. 15. Streamlines distributions of the diffuser following bleeding tube angles

4. Conclusion

Throughout the study, the effect of the bleeding tube is examined using the SST turbulence model to simulate the experimental 3-dimensional diffuser. The results show that the static pressure-recovery coefficient C_p has increased by 7% compared to the case with no bleeding tube. Additionally, the result of total pressure loss λ shows an 18.42% decrease, demonstrating a huge advantage of the bleeding tube. The validation of the computational process is examined with experimental results to prove the accuracy of the methodology. Based on those sets of data, the bleeding tube is applied with the parameters research.

Further works should be focused on investigating the real hybrid diffuser in a full combustion chamber combined with testing the effectiveness of the bleeding tube.

Acknowledgments

This work was supported by the Hanoi University of Science and Technology (HUST) under grant numbers T2021-TT-009 and T2021-PC-039.

References

[1] A. Klein, Characteristics of combustor diffusers, Progress in Aerospace Science, vol. 31, 1995, pp. 171–271. https://doi.org/10.1016/0376-0421(95)00006-K

[2] S. J. Stevens and G. J. Williams, The Influence of inlet conditions on the performance of annular diffusers, ASME. J. Fluids Eng., vol. 102(3), 1980, pp. 357–363. https://doi.org/10.1115/1.3240694

[3] F. Liepe, Efficiency of slender conical diffusers with the swirling flow, Maschineribautechnik, vol. 4, No. 8, 1960, pp. 405–412.

[4] A. M. Elkersh, A. H. Elgammal, and N. R. L. Maccallum, An experimental investigation of the performance of equiangular annular diffusers with

swirled flow, Proceedings of the Institution of Mechanical Engineers, Part C: Journal of Mechanical Engineering Science, vol. 199(4), 1985, pp. 293-297, https://doi.org/10.1243/PIME_PROC_1985_199_126_02

[5] M. Hanna, A. El-Kersh, R. Bassiouny, M. Gomaa, Air flow characteristics in an asymmetric plane diffuser under different inlet conditions, MJET, Minia Univ., El-Minia, Egypt, 2008.

[6] R. C. Adkins, D. S. Matharu, and J. O. Yost, The hybrid diffuser, ASME. J. Eng. Power, vol. 103(1), 1981, pp. 229–236. https://doi.org/10.1115/1.3230702

[7] A. J. Juhasz, Performance of a short annular dump diffuser using wall trailing-edge suction, NASA Technical Report, NO. NASA-TM-X-3093, 1974.

[8] A. J. Verdouw, Performance of the vortex-controlled diffuser (VCD) in an annular swirl-Can combustor flow path, in A. H. Lefebvre, ed., Gas turbine design problems, Hemisphere, Washington, DC, 1980, pp. 12–25.

[9] R. C. Adkins and M. H. Wardle, A method for the design of optimum annular diffusers of canted configuration, Journal of Engineering for Gas Turbines and Power, vol. 114(1), 1992, pp. 8–12. https://doi.org/10.1115/1.2906312

[10] A. D. Walker, P. A. Denman, and J. J. McGuirk, Experimental and computational study of hybrid diffusers for gas turbine combustors, Journal of Engineering for Gas Turbines and Power, vol. 126(4), 2004, pp. 717–725. https://doi.org/10.1115/1.1772403

[11] S. Obi, K. Aoki, and S. Masuda, Experimental and computational study of turbulent separating flow in an asymmetric plane diffuser, In Proc. 9th Symposium on Turbulent Shear Flows, 1993, pp. 305–312.

[12] ANSYS CFX 19.1 (2018) ANSYS CFX-Solver Theory Guide. ANSYS Inc.

[13] V. Chandavari and M. S. Palekar, Diffuser angle control to avoid flow separation, International Journal of Technical Research and Application, vol. 2(5), 2014, pp. 16-21.